

PAPER

Enhanced interfacial polarization in poly(vinylidene fluoride-chlorotrifluoroethylene) nanocomposite with parallel boron nitride nanosheets

To cite this article: Xuanhe Zhang *et al* 2020 *Nanotechnology* **31** 165703

View the [article online](#) for updates and enhancements.

Recent citations

- [Nanostructured boron nitride-based materials: synthesis and applications](#)
D. Gonzalez-Ortiz *et al*
- [Incorporation of elaborately Synthesized BNNs by a mild mechanical stirring process for the concurrent enhancement of thermal conductivity and dielectric breakdown strength of PVDF](#)
Jianping Chen *et al*




IOP | ebooks™

Bringing together innovative digital publishing with leading authors from the global scientific community.

Start exploring the collection—download the first chapter of every title for free.

Enhanced interfacial polarization in poly(vinylidene fluoride-chlorotrifluoroethylene) nanocomposite with parallel boron nitride nanosheets

Xuanhe Zhang¹, Hongyun Chen¹, Huijian Ye^{1,3}, Aiping Liu^{2,3} and Lixin Xu^{1,3} 

¹ College of Materials Science and Engineering, Zhejiang University of Technology, Hangzhou 310014, People's Republic of China

² Center for Optoelectronics Materials and Devices, Key Laboratory of Optical Field Manipulation of Zhejiang Province, Zhejiang Sci-Tech University, Hangzhou 310018, People's Republic of China

E-mail: huy19@zjut.edu.cn, liuaiping1979@gmail.com and gcsxlx@zjut.edu.cn

Received 11 November 2019, revised 11 December 2019

Accepted for publication 9 January 2020

Published 27 January 2020



Abstract

The miniaturization of electronics provides an opportunity for the polymer film capacitor due to its lightweight and flexibility. In order to improve energy density and charge–discharge efficiency of the film capacitor, the development of a polymer nanocomposite is one of the effective strategies, in which the distribution of the fillers plays a key role in the enhancement of the electrical energy capability. In this work, the few-layer boron nitride nanosheets (BNNSs) was exfoliated with assistance of the fluoro hyperbranched polyethylene-*graft*-poly(trifluoroethyl methacrylate) (HBPE-*g*-PTFEMA) copolymer as stabilizer, which was adsorbed on the surface of the nanosheets via a CH- π non-covalent interaction. The morphological results confirm the lateral size of $\sim 0.4 \mu\text{m}$ for resultant nanosheets with the intact crystal structure. The loading of 0.5 vol% BNNSs was embedded into poly(vinylidene fluoride-chlorotrifluoroethylene) (P(VDF-CTFE)) matrix by solution casting method, and then the nanocomposite film was uniaxial stretched to achieve the orientation of nanosheets in polymer host. The dielectric constant of stretching nanocomposite with ratio of 4 at 50 mm min^{-1} reaches 51.1 at 100 Hz with low loss as 0.016, while the energy density of 7.0 J cm^{-3} at 250 MV m^{-1} with charge–discharge efficiency of 56% is obtained in current nanocomposite film, which is attributed to the interfacial polarization as well as parallel nanosheets blocking the growth of electrical treeing branches. This strategy of the aligned nanosheets/polymer nanocomposite establishes a simple route to construct heterogeneity in polymer films with enhanced electrical energy capability for flexible capacitors.

Supplementary material for this article is available [online](#)

Keywords: P(VDF-CTFE), boron nitride nanosheets, hyperbranched copolymer, stretching, polarization, dielectric property, energy density

(Some figures may appear in colour only in the online journal)

³ Authors to whom any correspondence should be addressed.

Introduction

As one of the new-generation electrical storage technologies, polymer film capacitors have advantages of lightweight, processability, graceful reliability, and extremely fast discharge release, which is a promising candidate in the applications of microelectronic devices, artificial biological organs and sensors [1–4]. In general, the energy density (U_e) of linear polymer film is described as: $U_e = 1/2 \varepsilon_r \varepsilon_0 E_b^2$, where ε_r is relative permittivity, ε_0 the vacuum permittivity, and E_b is practical breakdown strength, from which the discharged U_e is determined by the relative permittivity and the breakdown strength of polymer dielectrics [5–8]. The biaxially oriented polypropylene (BOPP), a commercially available polymer film for capacitor, has an electrical density $U_e = \sim 2.3 \text{ J cm}^{-3}$ at 500 MV m^{-1} , which is ascribed to the low $\varepsilon_r = \sim 2.2$ at 100 Hz [9–11]. Thus, the increase of dielectric property for polymer film retaining high breakdown strength has become the effective solution to improve the energy capability of film capacitor [12–15].

The strategy of inorganic/organic nanocomposite has been suggested as a feasible route to enhance the electrical energy density of polymer capacitor [2, 8]. PVDF and its associated copolymers exhibit high dielectric constant compared with other polymers, which is recognized to be an ideal candidate for next-generation dielectric capacitors [2, 6, 16–19]. High- k ceramics were preferentially considered in PVDF-based nanocomposite to increase the dielectric constant, including BaTiO_3 (BT), $\text{Ba}_x\text{Sr}_{1-x}\text{TiO}_3$ (BST), $\text{Pb}_x\text{Zr}_{1-x}\text{TiO}_3$ (PZT) and $\text{CaCu}_3\text{Ti}_4\text{O}_{12}$ [20–24]. However, the large loading of ceramic particles is usually accompanied by the depression of breakdown field and mechanical property of polymer nanocomposite, in which the defects are ascribed to the agglomeration and the mismatch of the permittivity between high- k ferroelectric ceramics and polymer [5, 25].

The structural characteristic of boron nitride nanosheets (BNNSs) is isoelectric analogous to graphene, though exhibits electrical insulation, which is preferred for the energy storage of film capacitor under high electric field. The energy density $U_e = 7.25 \text{ J cm}^{-3}$ at 486 MV m^{-1} was obtained in 8 wt% hydroxyl groups modified BNNSs/PVDF nanocomposite owing to the improved compatibility and breakdown strength [26]. Additionally, the synergistic fillers of BNNSs and modified BT were incorporated into crosslinked PVDF (c-PVDF) matrix to suppress the leakage current, and $U_e = 5.2 \text{ J cm}^{-3}$ was achieved at 425 MV m^{-1} [27]. The prerequisite for high energy density of polymer nanocomposite is that the nanosheets are dispersed stably in the matrix with great compatibility, which is still a guide to improve the performance of energy storage devices in the future [28]. Compared with the nanoparticles and nanowires widely used in energy storage application, the paralleled 2D nanosheets perform as a number of microcapacitors inside composites [29–32]. When the array direction is perpendicular to the electric field, the nanosheets as barriers block the electrical treeing path [26, 33–35]. Developing an effective method to tailor the orientation of nanofillers retains a challenge for

now. The aligned array of reduced graphene oxide (rGO) in P(VDF-HFP) nanocomposite was obtained by repeatedly spin-coating technology, in which the shear force and the thickness were proposed as critical factors in the orientation of rGO nanosheets [36].

In our previous work, the orientation of few-layer graphene in P(VDF-HFP) was due to the combination of viscoelasticity for fluoropolymer and the entanglement effect between matrix and nanosheets during uniaxial deformation [37]. In order to further reduce the energy charge–discharge loss and improve practical breakdown strength, we applied insulating BNNSs as the parallel nanosheets in polymer composite via optimal stretching process to block the growth of electrical trees and enhance the energy capability. The fluoro hyperbranched HBPE-*g*-PTFEMA was employed to exfoliate the *h*-BN bulk into few-layer BNNSs as polymer stabilizer against the aggregation of nanosheets. The resultant flakes are dispersed uniformly in matrix due to the enhanced compatibility between P(VDF-CTFE) and nanosheets, which is ascribed to the fluoro segments of hyperbranched copolymer adsorbed on the surface of the BNNSs via CH- π interaction. The orientation of nanosheets in nanocomposite was achieved by in-plane uniaxial deformation, in which the aligned insulating nanoplates block the growth of electrical treeing branches. The BNNSs/P(VDF-CTFE) nanocomposite film under tensile ratio $R = 4$ with 50 mm min^{-1} exhibits the $U_e = 7.0 \text{ J cm}^{-3}$ at 250 MV m^{-1} , which directly benefits from interfacial polarization and the large content of electroactive phase. This work highlights a convenient strategy to develop the aligned few-layer BNNSs in PVDF-based nanocomposite for flexible film capacitors with high energy density.

Experimental

Materials

Hexagonal boron nitride (*h*-BN) powder with size of $\sim 1 \mu\text{m}$ (98%) was purchased from Sigma Aldrich, and P(VDF-CTFE) (9%–20% ratio of CTFE) with specific gravity $\sim 1.80 \text{ g cm}^{-3}$ was provided by Solvey. The *N,N*-dimethylformamide (DMF, $\geq 99.5\%$) was supplied from Wuxi Haisuo Biological Co. Hyperbranched polyethylene-graft-poly(trifluoroethyl methacrylate) copolymer (HBPE-*g*-PTFEMA) was synthesized by atom transfer radical polymerization (ATRP) using 2,2,2-trifluoroethyl methacrylate (TFEMA) with HBPE-Br as macroinitiator and Pd-diimine catalyst [38].

Preparation of BNNSs dispersion

The few-layer BNNSs was exfoliated from *h*-BN bulk in DMF with assistance of hyperbranched HBPE-*g*-PTFEMA copolymer that is adsorbed on the surface of the nanosheets via non-covalent CH- π interaction. Typically, 320.0 mg of *h*-BN powder and 320.0 mg of HBPE-*g*-PTFEMA were added into glass container with 80 ml of DMF. Then, the mixture

Table 1. Preparation for BNNSs/P(VDF-CTFE) nanocomposites with different stretching conditions at 80 °C.

Sample	Stretching ratio	Stretching rate (mm min ⁻¹)
1	$R = 0$	0
2	$R = 2$	50
3	$R = 4$	
4	$R = 5$	
5	$R = 6$	
6	$R = 4$	3
7		10
8		20
9		200

was sonicated for 48 h at room temperature with a continuous flow of water. Subsequently, the initial product was centrifuged at 3000 rpm for 20 min in order to remove the residual *h*-BN particles. The supernatant was carefully collected and further vacuum filtered by nylon 66 membrane with 200 nm to eliminate the excess HBPE-*g*-PTFEMA. Finally, the white filter cake was dispersed in DMF under sonication, and the stable BNNSs dispersion with concentration $C_B = 1.0 \text{ mg ml}^{-1}$ was obtained.

Preparation of stretching BNNSs/P(VDF-CTFE) nanocomposite

The P(VDF-CTFE) nanocomposite film with 0.5 vol% BNNSs was prepared via simple solution casting. P(VDF-CTFE) powders were initially stirred in DMF at room temperature for 2 h. After the addition of the BNNSs dispersion, the suspension was stirred for 15 min, which was then poured on the glass plate and dried at 80 °C for 10 h. After peeled off the substrate, the free-standing nanocomposite film with a thickness of 40 μm was further annealed at 120 °C for 10 h to eliminate the residual solvent and increase the crystallinity. The parallel array of nanosheets was accomplished by uniaxial stretching on Instron 5569 with an isothermal environment. Briefly, the pre-stretched sample was tailored to strips and held with fixtures in a temperature controlled component at 80 °C for 10 min to achieve thermal equilibrium of the film. Different drawing ratios (*R*) and rates were performed to drive the nanosheets aligning along the deformation direction. The detailed preparation parameters of the various samples are listed in table 1.

Characterizations of BNNSs

High-resolution transmission electron microscopy (HRTEM, 300 kV JEM-100CX II electron microscope, FEI) images were taken for the morphologies of nanosheets. The sample for HRTEM was prepared by dropping the BNNSs dispersion on the carbon-coated copper grid and removing the solvent with an infrared lamp prior to observation. Raman spectra of nanosheets were carried out on Renishaw Invia with 532 nm

excitation wavelength. In order to estimate the adsorption of HBPE-*g*-PTFEMA on the surface of the nanosheets, x-ray diffraction (XRD) patterns of BNNSs were collected on the X'Pert PRO apparatus of Shimadzu (Cu $K\alpha$ $\lambda = 1.54\text{\AA}$) from 10° to 80° with 4° min⁻¹, and the free copolymer was filtered before testing. Fourier transform infrared spectra (FT-IR, Nicolet 6700, TA) were employed with the measurement range from 4000 cm⁻¹ to 400 cm⁻¹ with increment of 2 cm⁻¹. The surface morphology of BNNSs was examined by atomic force microscopy (AFM, Bruker) with tapping mode. The sample was deposited on the mica substrate and dried vacuum at 80°C prior to characterization.

Characterization of nanocomposite films

XRD was used to evaluate the crystal structure of BNNSs/P (VDF-CTFE) nanocomposite film with the scanning range from 5° to 65° with the rate of 4°/min. FT-IR spectra from 4000 cm⁻¹ to 650 cm⁻¹ with increment of 0.5 cm⁻¹ were carried out to calculate the relative content of the β -phase in the nanocomposite. AFM technology was applied to examine the surface morphology of nanocomposite film with scanning range of 10 $\mu\text{m} \times 10 \mu\text{m}$. The cross-sectional morphologies of samples were observed via field emission scanning electron microscopy (SEM, Nano SEM 450 equipment, FEI), and the SEM sample was frozen-fractured in liquid nitrogen and spray-coated with thin Pt conductive layer before characterization. The dielectric properties of the nanocomposite films were tested at frequency from 10² to 10⁶ Hz with 0.5 V rms on Agilent 4294A LCR impedance analyzer. The electric displacement loops were measured at 100 Hz by TREK 609B-3-K-CE equipment from Radiant Technologies. The Pt layer electrode of 0.0707 cm² was sprayed on both sides of the film prior to examination.

Results and discussion

Morphology and nanostructure of BNNSs

The high-quality few-layer BNNSs were exfoliated from *h*-BN powder with assistance of hyperbranched polyethylene (HBPE) as stabilizer in common organic solvents [39]. During the liquid-phase exfoliation HBPE is adsorbed on the surface of nanosheets by non-covalent CH- π interaction, which retains the stable dispersion of few-layer nanosheets against re-stacking due to its hyperbranched topology structure. In order to enhance the compatibility between nanosheets and fluoropolymer matrix, we synthesized the hyperbranched HBPE-*g*-PTFEMA copolymer by tailoring the fluoro PTFEMA segments on the functional ends of HBPE via ATRP technique [38]. The process of one-step exfoliation and simultaneous surface modification of BNNSs are illustrated schematically in figure 1. The received BNNSs were dispersed stably in DMF, and the dispersion was added into P(VDF-CTFE) solution to prepare the BNNSs/P(VDF-CTFE) nanocomposite film via solution casting method.

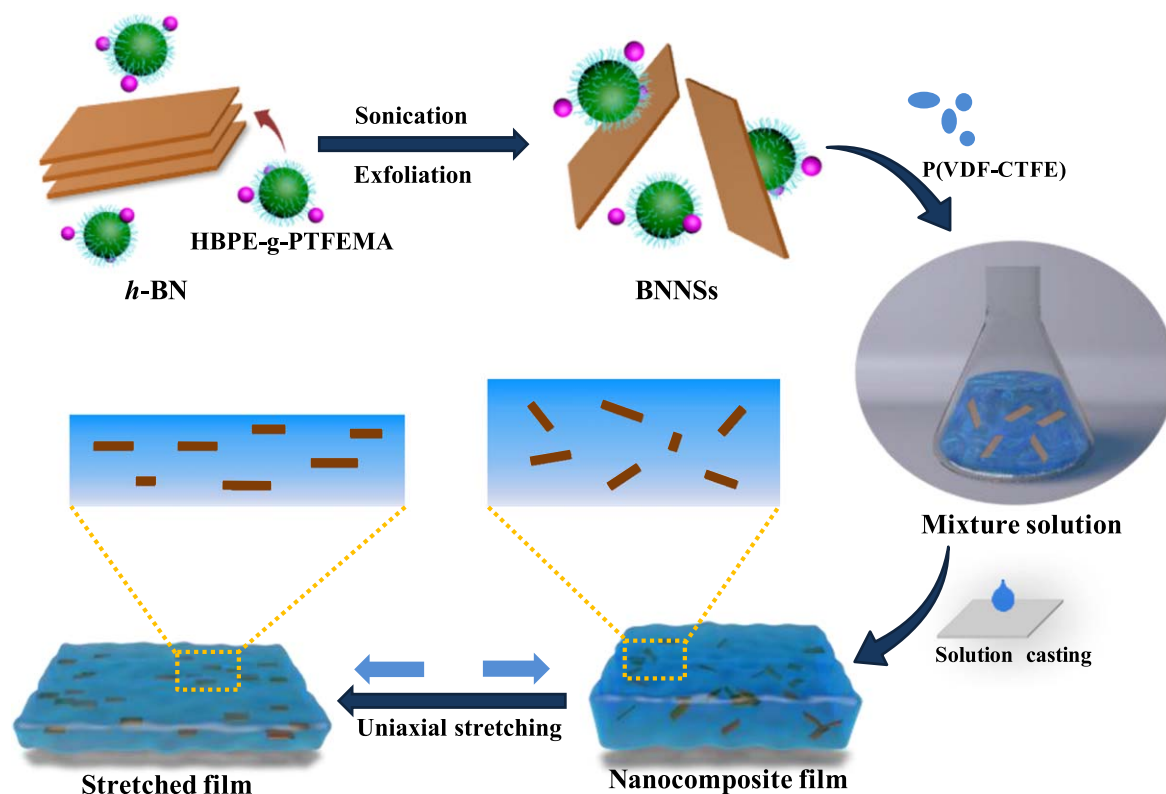


Figure 1. Schematic illustration for liquid-phase exfoliation of BNNSs in DMF with assistance of HBPE-g-PTFEMA and subsequently the preparation of stretching BNNSs/P(VDF-CTFE) nanocomposite film.

Finally, the flexible film was uniaxially stretched at a constant temperature to tune the orientation of nanosheets along the direction of deformation, which is ascribed to the polymer intrinsic viscoelasticity and the strong van der Waals forces between matrix and fluoro copolymer attached on the surface of nanosheets [37].

The morphology and crystal structure of the resultant BNNSs are shown in figure 2, indicating the received BNNSs with a smooth surface. It is suggested that the specific layer number of nanosheets could be counted through the curled edge from HRTEM image inset figure 2(a), which reveals that the number of layers is statistically in the range 4–8 with the lateral dimension of $\sim 0.4 \mu\text{m}$. The corresponding selected area electron diffraction (SAED) (inset of figure 2(b)) exhibits clearly symmetric hexagonal diffraction ring with the reflections of (010), (110) and (020) crystalline planes [40]. The six-membered ring structure in figure 2(b) are observed as a typical atomic map, which identifies the intercal lattice structure of nanoplate. The surface morphology of nanosheets was examined by AFM, and the image is displayed in figure 2(c), from which the flakes exhibit smooth surface. The corresponding thicknesses from the height profiles in figure 2(d) are 1.5, 1.4 and 1.6 nm, which is consistent with the above TEM results. Furthermore, the Raman spectra in figure 2(e) include the E_{2g} characteristic peak around 1366 cm^{-1} for both *h*-BN and BNNSs samples due to the B–N = B vibration mode. Compared with the curve for *h*-BN bulk, the peak of few-layer nanosheets in figure 2(f) is surfaced a red shift of 2 cm^{-1} , which has been proposed as the

variation caused by the few-layer BNNSs [41]. Meanwhile, the full width at half maximum (FWHM) decreases from 13.6 cm^{-1} for *h*-BN to 10.1 cm^{-1} for the received BNNSs, which also confirms that the few-layer nanosheets have been successfully exfoliated from bulk *h*-BN with the assistance of HBPE-g-PTFEMA copolymer [42].

The obtained BNNSs are dispersed stably in the DMF because the hyperbranched copolymer adsorbs onto the surface of the nanosheets by the CH- π interactions against the flakes re-stacking. The attachment of fluoro HBPE-g-PTFEMA copolymer was characterized by the XRD patterns and FT-IR spectra that are shown in figures 2(g) and (h), respectively. The pattern of *h*-BN bulk presents three distinct peaks associated with crystal plane of (002), (100) and (104). However, the intensities for these peaks are weakened in the curve of the BNNSs with an amorphous broad peak, which is assigned to the characteristic shape of the fluoro copolymer. Similarly, the FT-IR spectrum of the nanosheets appears several new peaks at 2930 , 1752 and 1170 cm^{-1} , which belong to the stretching vibrations of C–H, C=O and C–O in the fluoro hyperbranched copolymer [38]. These results prove the presence of HBPE-g-PTFEMA copolymer on the surface of nanosheets that is accomplished with CH- π non-covalent interaction [39]. The terminal fluoro segments will yield compatible BNNSs/P(VDF-CTFE) nanocomposite, which accounts for the enhancement of dielectric property and electrical energy capability of polymer film.

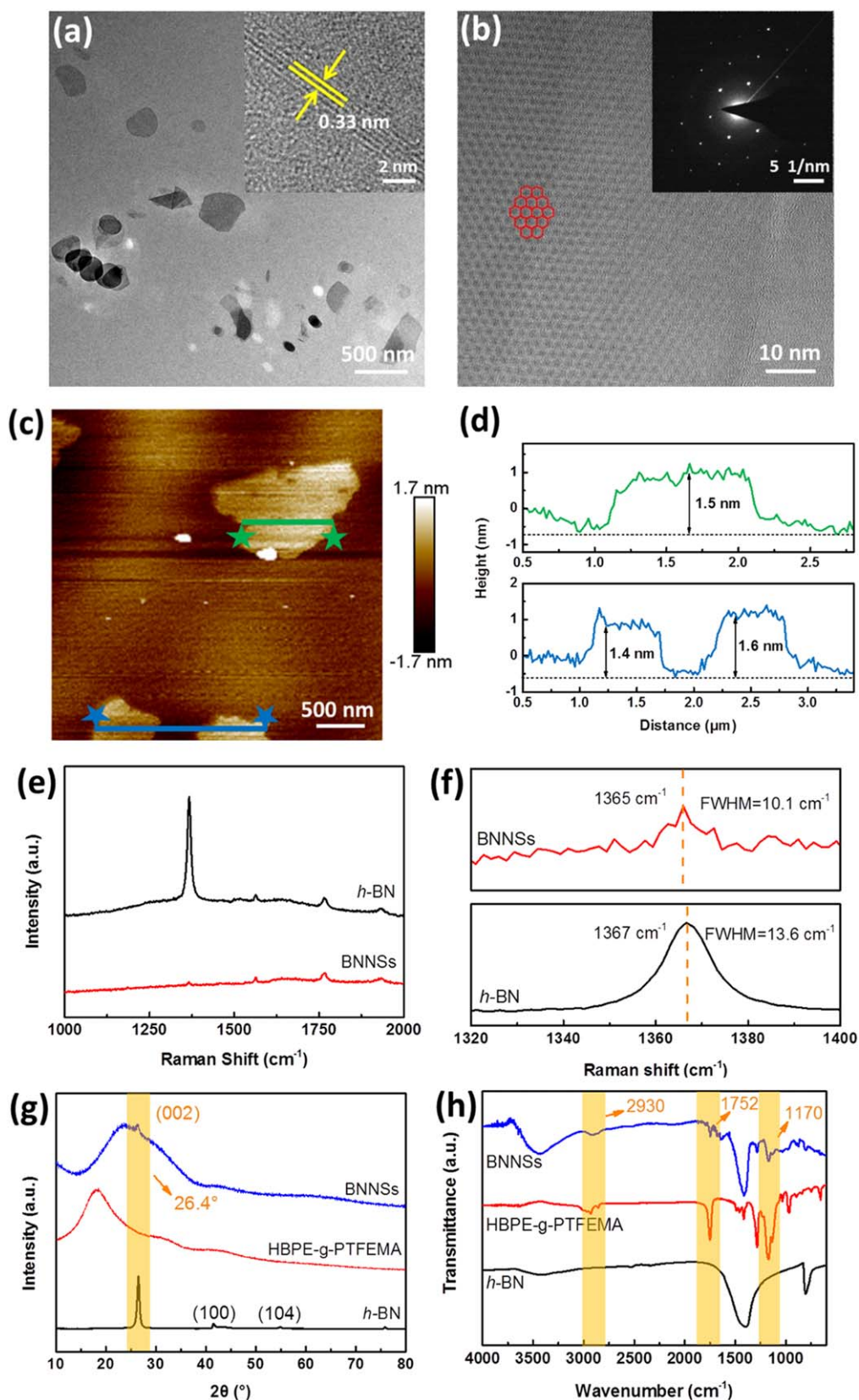


Figure 2. Morphology and nanostructure of BNNSs obtained by liquid exfoliation: (a) HRTEM image, inset is the curled edges, (b) typical atomic HRTEM image, the inset shows the corresponding electron-diffraction pattern, (c) AFM image, (d) the corresponding height profile in AFM image, (e) and (f) the Raman spectra, (g) XRD curves, and (h) FT-IR spectra.

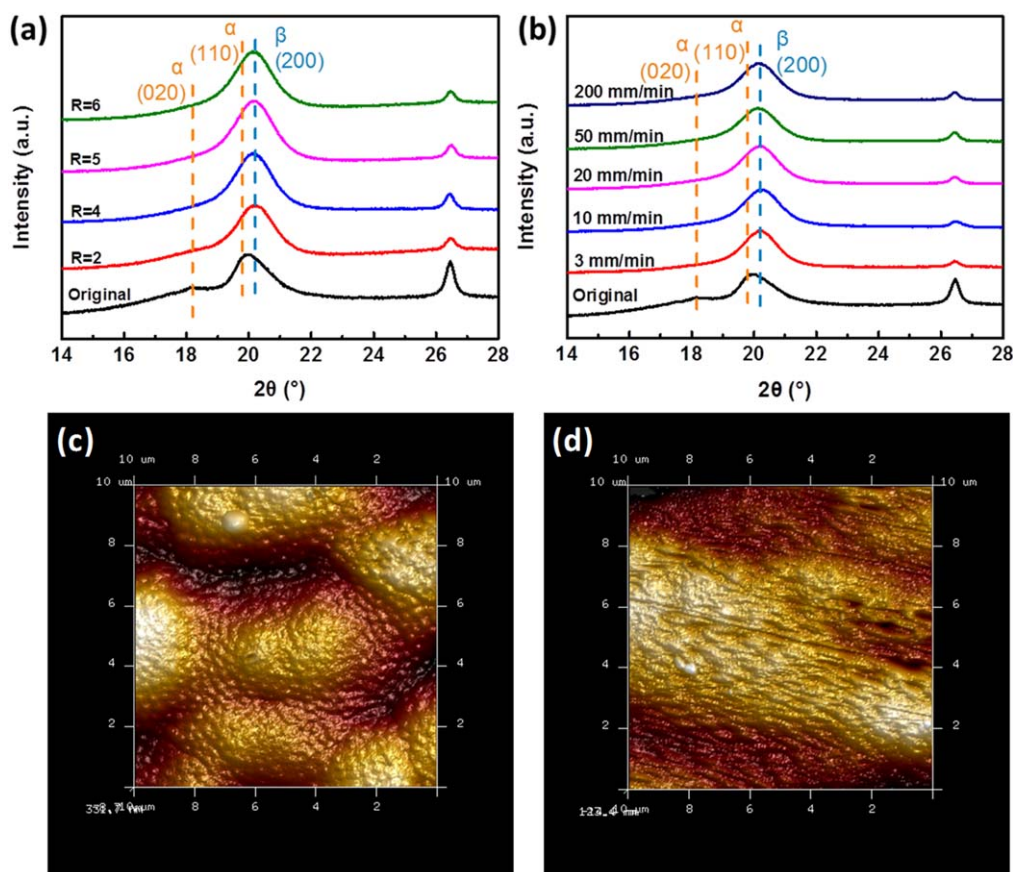


Figure 3. XRD patterns for BNNSs/P(VDF-CTFE) nanocomposite films: (a) different ratios at 50 mm min⁻¹, (b) different stretching speeds at $R = 4$; the surface morphologies by AFM: (c) original film and (d) stretching film with $R = 4$ at 50 mm min⁻¹.

Electroactive phase transition in nanocomposite

XRD technology is often applied to distinguish the different phases of PVDF-based semi-crystalline polymers [3, 35]. As displayed in figure 3(a), the original film has a weak characteristic peak at 18.2°, which is corresponding to the (020) plane of the *non*-polar α -phase, while another peak at $2\theta = 19.8^\circ$ belongs to the (110) plane of the α -phase. The strong diffraction at 19.8° for the original film approaches the peak of (200) plane at 20.2° for the electroactive β -phase due to the heterogeneous nucleation of the BNNSs and orientation effect of macromolecular chain [19]. The diffraction at 18.2° for α -phase is substantially disappeared after deformation, which strengthens the transition from α -phase to β -phase under uniaxial force [17, 43]. The peak at 26.4° is assigned to the (002) crystal plane for boron nitride, and its attenuation implies partial dilution of nanosheets in the matrix as in-plane deformation. The crystallinity was estimated from the XRD curve, and the result is shown in supplemental information figure S1, which is available online at stacks.iop.org/NANO/31/165703/mmedia. The crystallinity has been enhanced significantly after stretching due to the orientation of the macromolecular chain along the force direction. In addition, the surface morphologies of the nanocomposite films taken by AFM are presented in figures 3(c) and (d), from which the distinct spherulite morphology is observed in the original film. The external mechanical force induces the necking

phenomenon that the inner molecular chains are rearranged along the force direction transforming into all-*trans* conformation (*TTTT'*) for the β -phase [6].

In order to evaluate quantitatively the relative content of the β -phase, the characteristic peaks for different crystal phases examined by the FT-IR spectra are shown in the figure 4. The peak at 763 cm⁻¹ is assigned to the bending vibration of the CF₂ unit on the molecular backbone belonging to the α -phase, and the peak at 836 cm⁻¹ is regarded as the band for the β -phase, which is corresponding to the rocking mode of CH₂ and CF₂ asymmetric stretching [44]. After the stretching improvement, the intensity of peak for the β -phase is enhanced accompanying with a slight decrease of band at 763 cm⁻¹ for α -phase. This trend echoes the results of XRD, implying the phase transition during the uniaxial deformation. Assuming the infrared absorption complies with Lambert Beer's law, the specific content of the β -phase ($F(\beta)$) is estimated by the following expression [44]:

$$F(\beta) = \frac{X_\beta}{X_\alpha + X_\beta} = \frac{A_\beta}{(K_\beta/K_\alpha)A_\alpha + A_\beta}, \quad (1)$$

where A_α and A_β represents the absorbencies at 763 and 836 cm⁻¹; K_α and K_β are the absorption coefficients at the respective wavenumbers, which are 6.1×10^4 and 7.7×10^4 cm² mol⁻¹, respectively. The relative contents of β -phase under different stretching conditions are illustrated in figures 4(c) and (d). In the pre-stretched 0.5 vol% BNNSs/P

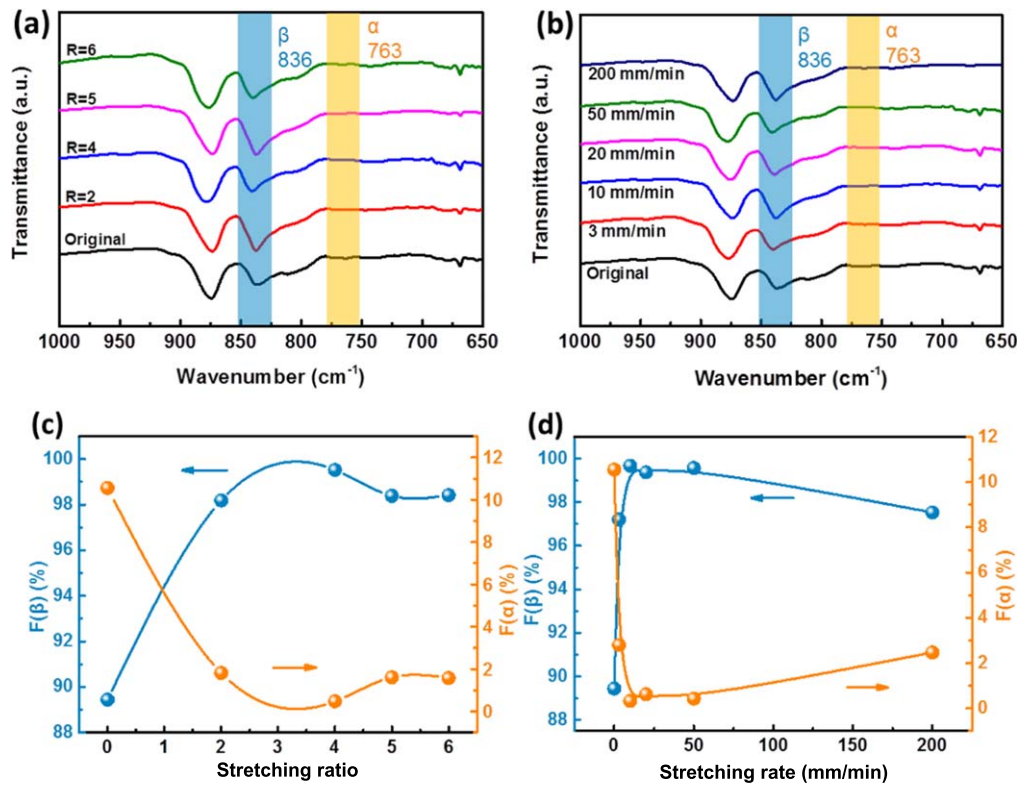


Figure 4. FT-IR spectra for stretching BNNs/P(VDF-CTFE) nanocomposite films: (a) different ratios at 50 mm min^{-1} , (b) different stretching speeds at $R=4$; corresponding contents of β -phase in stretching nanocomposite films: (c) different ratios at 50 mm min^{-1} , (d) different stretching rates at $R=4$.

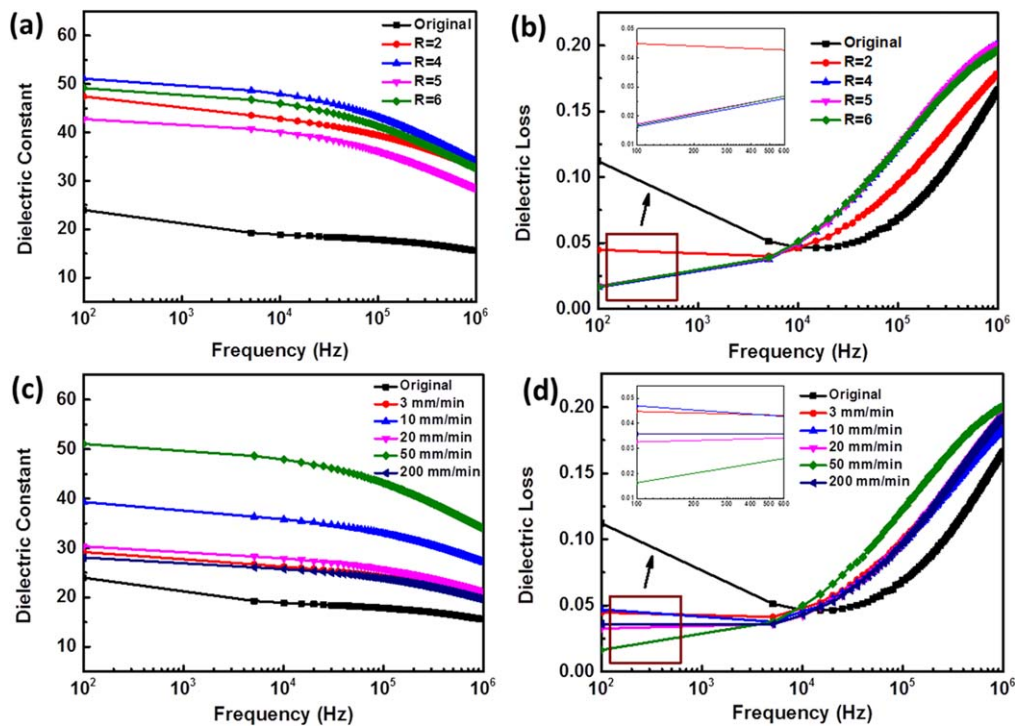


Figure 5. (a) Dielectric constant and (b) dielectric loss of BNNs/P(VDF-CTFE) nanocomposite films with various ratios at 50 mm min^{-1} , (c) dielectric constant and (d) dielectric loss of nanocomposite films with different stretching speeds with $R=4$.

(VDF-CTFE) nanocomposite, the $F(\beta) = 88\%$ is reached due to the combination of heterogenous nucleation of nanosheets and thermal annealing effect. After the stretching treatment, the content of β -phase increases up to 98% as ratio $R = 4$. However, under high rate the deformation of molecular chain appears to be sluggish because the segments have not been aligned completely within limit time [45].

Dielectric property and energy storage of nanocomposite

The dielectric property of stretching nanocomposite films under the frequency from 10^2 to 10^6 Hz are illustrated in figure 5. There is a significant improvement for the dielectric constant of stretching nanocomposite compared with the original sample. With the stretching ratio and rates increases, the dielectric constant is enhanced and the maximum dielectric constant $\epsilon' = 51.1$ is achieved at $R = 4$ with the rate of 50 mm min^{-1} , which is 2.1 times higher than $\epsilon' = 24.3$ for original nanocomposite film. When the uniaxial external force is applied, the difference of stress distribution occurs between the nanosheets and the polymer matrix, which affects the molecular chain transition preferentially starting from the adjacent to the nanosheets [17]. This phenomenon forms an oriented inorganic-organic route consisting of structural units that some macromolecular segments extend from the nanoplates. This lateral path prevents carriers diffusing in the direction of the electric field and depresses the flow efficiency of charges, which contributes to the improvement of the dielectric reliability [37]. The falling tendency of the stretching film at frequency of $10^4 \sim 10^6$ Hz suggests the dominating contribution of polarized dipoles under high frequency [46].

As shown in the figures 5(b) and (d), under low frequency the dielectric loss ϵ'' of the stretching film is significantly decreased, e.g. $\epsilon'' = 0.016$ at 100 Hz. The loss rises sharply as the frequency increases from 10^4 to 10^6 Hz, which is induced by the orientation of C-F dipoles. The loss is a critical factor for film capacitor, which is mainly induced by the ferroelectric switching loss and electrical conduction of polymer film. In some polymer composite systems, the loss tangent is described as following formula [35]

$$\epsilon'' = \epsilon''_{\text{con}} + \epsilon''_{\text{inter}} + \epsilon''_{\text{dipole}}, \quad (2)$$

where ϵ''_{con} , $\epsilon''_{\text{inter}}$ and $\epsilon''_{\text{dipole}}$ represent loss resulting from conduction, interfacial polarization and dipole polarization, respectively. The interaction between nanosheets and matrix is strengthened due to the presence of fluoropolymer and phase transition starting from the periphery of the nanosheets. The dipole polarization becomes the primary factor on the overall dielectric loss [47]. Besides, the optimum stretching improvement leads to high orientation and packing density of macromolecular segments.

The set of unipolar hysteresis displacement loops versus electric field (P-E) at 250 MV m^{-1} for typical nanocomposite films with various stretching conditions are displayed in figures 6(a) and (b). The electric displacement is improved after the stretching process, which is mainly attributed to the

large content of the electroactive phase and the interfacial interaction. The detailed hysteresis loops as a function of electric field for stretching films are shown in figure S2. To examine quantitatively the improvement of electric displacement, the extracted maximum polarizations (P_{max}) are plotted in figures 6(c) and (d), in which a significant leap in P_{max} is observed when the rate is increased from 10 to 20 mm min^{-1} . This phenomenon also supports the dominance of dipole polarization. Due to the influence of entropy, the slow stretching speed induces the macromolecular segments around the nanosheets to be a transition state that tends to recover and introduce some defects in the nanocomposite film. The macromolecular chain in the converted β -phase cannot escape from the amorphous region. As the deformation progresses, it is like a knotted yarn ball becomes tighter, and eventually leads to incomplete polarization under the high field [48].

The breakdown strength of stretching BNNSs/P(VDF-CTFE) nanocomposite could be dissected by a two-parameter Weibull equation [8, 14, 49]:

$$P(E) = 1 - \exp(-(E/E_b)^m), \quad (3)$$

where $P(E)$ is the cumulative probability of electrical failure, E the experimental electric field strength, E_b a typical strength with probability of breakdown as 63.2%, and shape parameter m is related to the linear regressive fit of the distribution, which could evaluate the dielectric reliability. The fitted lines of the typical samples are presented in figure 6(e) with the inset corresponding E_b and m values. The high m value after deformation indicates that the film retains graceful dielectric reliability and the stretching process does not impair the compatibility between the nanosheets and P(VDF-CTFE) matrix due to the attachment of fluoropolymer. The breakdown possibility of nanocomposite versus applied electric field is calculated inset figure 6(e). The inflection points of the stretching films are centered at $\sim 250 \text{ MV m}^{-1}$, which is higher than that of the original film of $\sim 150 \text{ MV m}^{-1}$. The Weibull breakdown strength E_b is extracted separately and plotted in figure 6(f) for an intuitive comparison. The E_b value of the stretching film generally increases and reaches maximum of 291.8 MV m^{-1} , 84.9% higher than that of the original film, which is mainly ascribed to the inhibition of electrical treeing by the rearranged nanosheets in the nanocomposite [26]. The cross-sectional morphology by SEM image in figure S3 shows no obvious crack in stretching film. During mechanical improvement, the BNNSs are redistributed as parallel array perpendicular to the electric field along with the orientation of the macromolecular chains, which prevents the extension of the electrical branches. In addition, the few-layer nanosheets obtained by liquid exfoliation have low lattice defects, and the surface-adsorbed fluoropolymer improves the compatibility with the matrix, thus the electrical trees are difficult to bypass the BNNSs [33].

The discharged energy density of BNNSs/P(VDF-CTFE) nanocomposite film is estimated from the P-E loop by

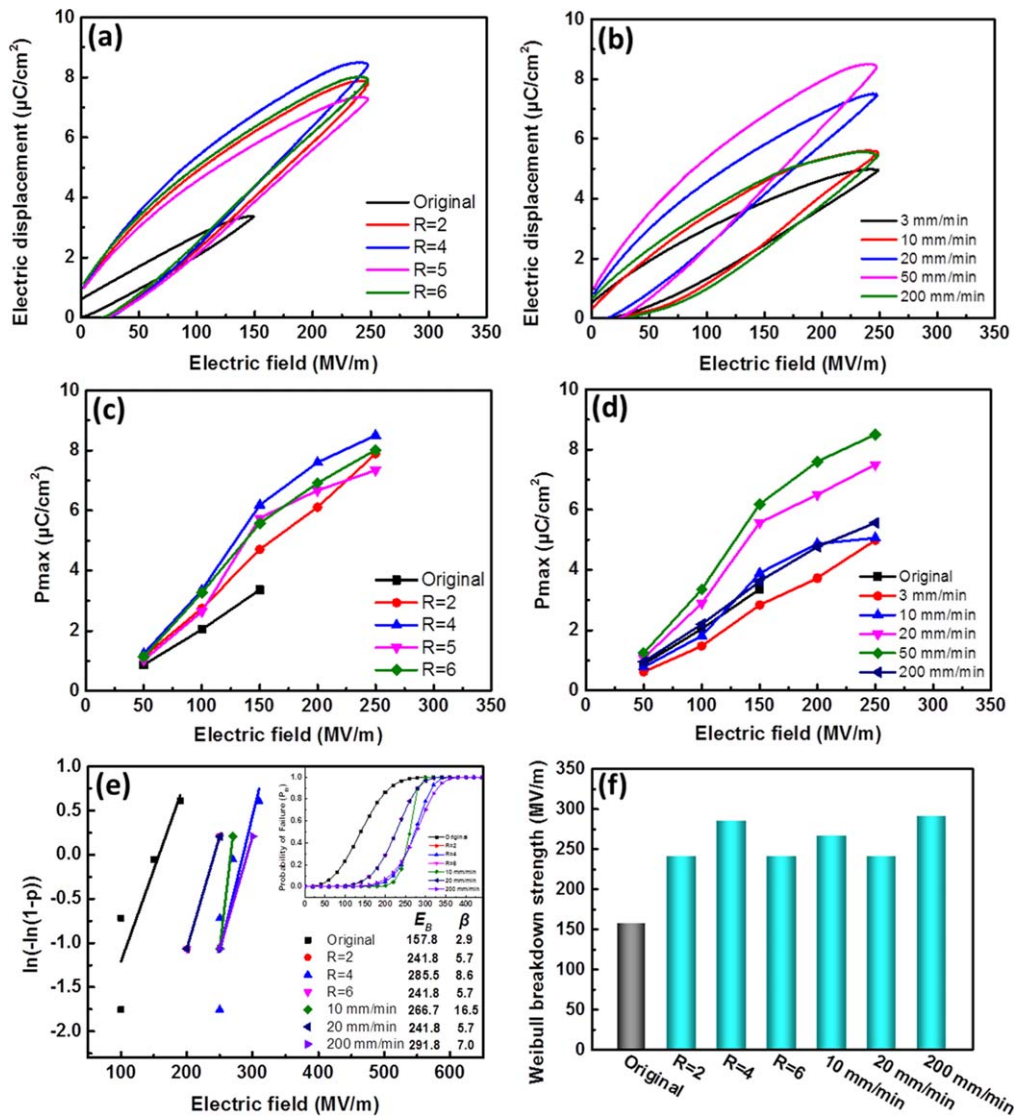


Figure 6. The typical unipolar hysteresis loops of stretching BNNSs/P(VDF-CTFE) nanocomposite films: (a) various ratios at 50 mm min⁻¹, (b) different rates with $R = 4$; the maximum polarizations of (c) various ratios at 50 mm min⁻¹ and (d) different rates with $R = 4$; (e) Weibull distribution, the inset is failure probability versus applied electric field, and (f) Weibull breakdown strength.

the following formula:

$$U_e = \int E dD, \quad (4)$$

where D and E are the corresponding polarization and applied external field, respectively. The released energy density and charge-discharge efficiency of BNNSs/P(VDF-CTFE) nanocomposite films are shown in figure 7. The stretching nanocomposite film with 50 mm min⁻¹ at $R = 4$ exhibits the highest energy density $U_e = 7.0 \text{ J cm}^{-3}$ with charge-discharge efficiency $\eta = 56.1\%$ at 250 MV m⁻¹. The effect of stretching rate on the discharged energy density of nanocomposite film is plotted in figure 7(c). Under high stretching rate the extreme speed induces the electroactive phase to be tightly wrapped by the molecular chain that undergoes phase transformation, leading to insufficient dipole polarization accompanied by great friction. The electric field is similar to a force that initiates dipole rotation. The low field strength mainly enables the β -phase to prevail the surrounding barrier.

When the electric field strength reaches a certain value, the loss induced by the relatively free rotation of the dipole becomes the domination effect [50]. The comparison of electrical capability of stretching BNNSs/P(VDF-CTFE) developed in this study and selected reported PVDF-based nanocomposites is listed in table 2. The stretching nanocomposite film exhibits relatively high energy density and charge-discharge efficiency, which is primary for the energy storage device where the weight and the occupation are mainly concerned.

In order to clarify the effect of the aligned BNNSs on the diffusion of electrical treeing, the field distribution model of vertical cross-section sample is established by finite element simulation. As presented in figures 8(a) and (b), the applied voltage on the sample with thickness of 20 μm is 3000 V as illustrated in electrical potential distribution in figure S4. Here we set the dielectric constant of BNNSs and P(VDF-CTFE) as 5 and 13, respectively, and the electrical conductivity is

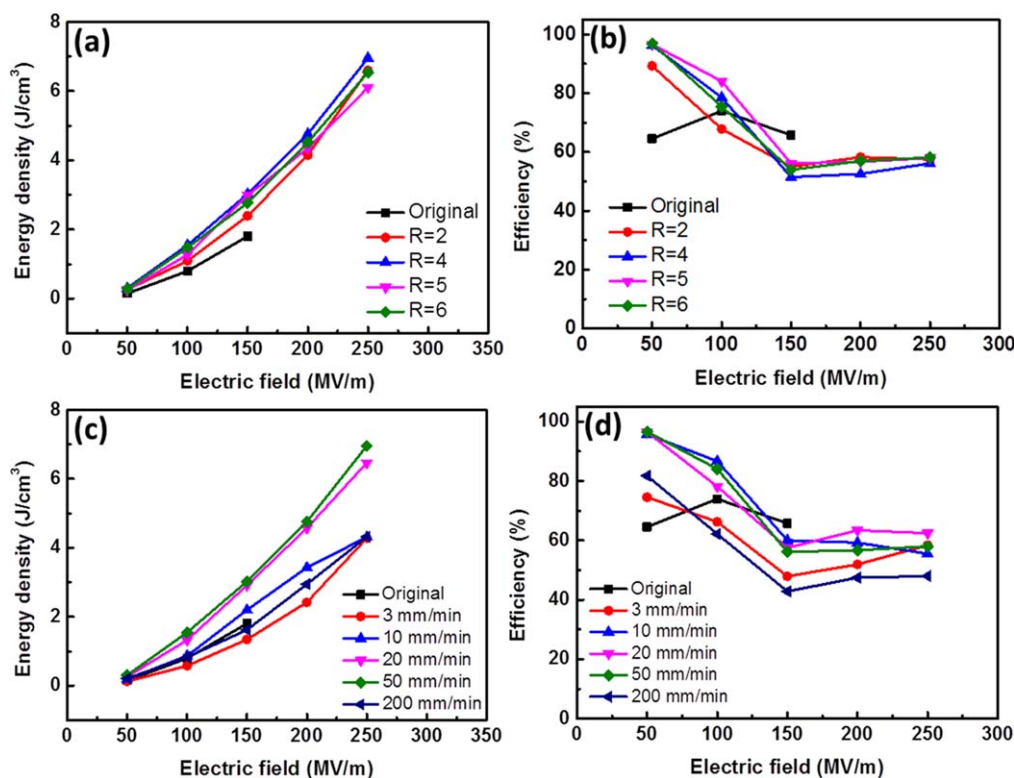


Figure 7. (a) Discharged energy density and (b) charge–discharge efficiency of BNNSs/P(VDF-CTFE) films with various stretching ratios, (c) discharged energy density and (d) charge–discharge efficiency of films with different stretching rates.

Table 2. Comparison of electrical energy storage in PVDF-based nanocomposites developed here with those in the literature.

Samples	ϵ' (1 kHz)	ϵ'' (1 kHz)	ΔE (MV m ⁻¹)	U_e (J cm ⁻³)	η (%)	References
Stretching 0.5 vol% BNNSs/P(VDF-CTFE) (50 mm min ⁻¹ at $R = 4$)	49	0.03	250	7.0	56.1	This work
1 vol% TiO ₂ -g-PMMA/P(VDF-HFP)	10	0.03	500	10.8	47	[51]
10 vol% PZT/PVDF	12	0.03	250	6.4	40	[52]
0.02 wt% Au nanorods/P(VDF-CTFE)	8.8	—	230	4.6	62.2	[53]
3 vol% NaNbO ₃ @PDA@Ag nanowires/PVDF	10	0.025	485	16	62.8	[54]
3 vol% BT nanofibers/P(VDF-HFP)	18	0.07	300	8.6	57	[55]
5 wt% BT/6 wt% BNNSs/c-PVDF	10.8	0.05	425	5.2	50	[27]
0.1 vol% Graphene/P(VDF-CTFE)	18.2	0.04	250	4.6	62	[56]
2.5 vol% Nd-doped BT/PVDF	16.5	0.05	350	7.9	40	[57]
5 wt% BT@BN/PVDF	11.5	0.03	250	3.6	87	[58]
0.5 mol l ⁻¹ TiO ₂ nanowire array/PVDF	15	0.03	505	8.9	—	[59]
12 vol% methacrylate-butadiene-styrene/PVDF	8.1	0.02	535	9.8	—	[60]
3.6 vol% BT@Al ₂ O ₃ nanofibers/PVDF	13	0.02	420	11.5	62.5	[61]

assigned to 10^{-17} S m⁻¹ for BNNSs and 10^{-13} S m⁻¹ for matrix in this simulation. It is observed that the partial voltage is accumulated on the nanosheets, which preferentially spreads to the edges of nanoplates. Compared with the homogeneous nanocomposite film, the local field extends along the orientation direction of the nanosheets in the stretching nanocomposite, which implies that the BNNSs array perpendicular to the applied field direction guides the lateral propagation of the electrical treeing, which is illustrated schematically in figure 8(c). Similarly, the field strength in the middle of parallel nanoplates is higher than

that of nanocomposite with isotropic dispersion because of the head-on collision effect between the electrical branches and the oriented nanosheets. The simulation results are consistent with the experimental data, which further confirms that the oriented nanosheets block the diffusion of charge carriers and improve the resistance of electrical treeing inception [26].

The electric field is re-allocated in the aligned nanosheets/polymer nanocomposite based on the difference of dielectric property and the continuity of electric displacement at the adjacent interfacial region. The term breakdown is employed to describe a dynamic transfer when the current

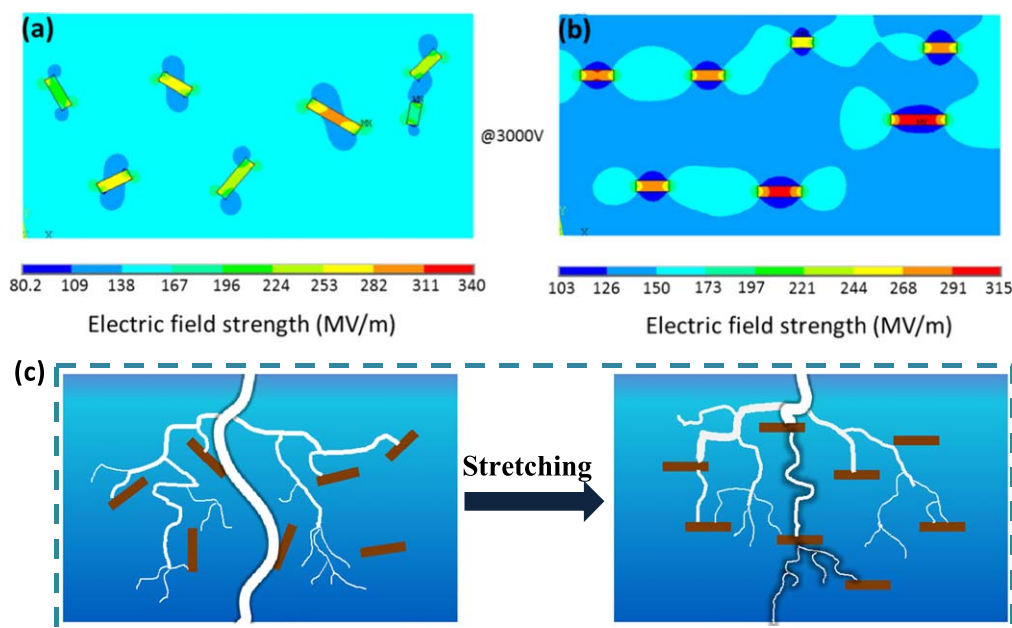


Figure 8. The distribution of electric field in BNNSs/P(VDF-CTFE) nanocomposite by finite element simulation: (a) random dispersion of nanosheets in pre-stretched film, (b) aligned nanosheets in stretching film, and (c) schematic view of electrical treeing growth in nanocomposite film before and after stretching. The thickness of the film is 20 μm , and the applied electrical voltage is 3000 V.

increases dramatically with small voltage variation. The breakdown failure occurs in the polymer insulator is usually very fast, and it is destructive that makes irreversible effects in the material. Compared with the intrinsic breakdown, in practical case, the engineering breakdown is determined by the polymer morphology, chemical impurities, and defects in the film. Under high field the collision between the hot electrons with trapped electrons leads to avalanche or impact-ionization breakdown [18]. The distribution of nanosheets is proposed as an important factor to determine the efficiency of transportation for charge carriers. The anisotropic composite has been evidenced as an effective strategy to reduce the nonlinear conduction, which is a dominate loss mechanism under high field, and retains the dielectric breakdown strength in the heterogeneous system [22]. The orientation of nanosheets contributes to the prolonged path distance, in which the tortuous path depends on the layer aggregation and alignment of nanofillers. The electron trapping sites with a range of barriers for electron transfer are redistributed perpendicular to the external field direction. When the applied field reaches a critical value to accelerate carriers flowing towards the adjacent trapping that is perpendicular to the field direction, which increases the path of electrical branches and thus, improves the dielectric reliability. The space charge conduction and the accumulation of local field are associated with the anisotropic state of nanosheets in the polymer dielectrics. The alignment of nanosheets in nanocomposite sheds a light on mechanism of electrical breakdown, and paves the path to the high energy density and charge-discharge efficiency of polymer nanocomposite for flexible film capacitor.

Conclusions

In summary, BNNSs/P(VDF-CTFE) nanocomposite film with high dielectric property and electrical energy capability has been prepared by uniaxial stretching improvement. The BNNSs was exfoliated with assistance of HBPE-g-PTFEMA as polymer stabilizer, which was adsorbed on the surface of nanosheets via CH- π non-covalent interaction. The presence of fluoro copolymer enhances the compatibility between nanosheets and polymer matrix. The orientation of macromolecular segments simultaneously drives the BNNSs to be distributed in a direction parallel to the force, which would block the development of the electrical treeing under high field. The released energy density of stretching nanocomposite film reaches 7.0 J cm^{-3} at 250 MV m^{-1} , which benefits from large content of electroactive phase and interfacial polarization. This work establishes a feasible strategy to improve the compatibility in oriented nanosheets/polymer nanocomposite with high electrical energy capability for flexible film capacitors.

Acknowledgments

The financial support from the National Natural Science Foundation of China (51707175), Natural Science Foundation of Zhejiang Province (LTZ20E070001, LY18B040005), and China Postdoctoral Science Foundation (2018M640572) is greatly appreciated.

ORCID iDs

Lixin Xu  <https://orcid.org/0000-0001-9196-2763>

References

- [1] Li Q, Liu F, Yang T, Gadinski M R, Zhang G, Chen L-Q and Wang Q 2016 Sandwich-structured polymer nanocomposites with high energy density and great charge-discharge efficiency at elevated temperatures *Proc. Natl Acad. Sci. USA* **113** 9995–10000
- [2] Prateek, Thakur V K and Gupta R K 2016 Recent progress on ferroelectric polymer-based nanocomposites for high energy density capacitors: synthesis, dielectric properties, and future aspects *Chem. Rev.* **116** 4260–317
- [3] Zhu W, Ma J, Nan X, Lartey P O and Yang Y 2019 Study on dispersion of reduced graphene oxide on physical performance of polyvinylidene fluoride composites by hansen solubility parameters *Colloid Polym. Sci.* **297** 213–24
- [4] Tian M, Zhang J, Zhang L, Liu S, Zan X, Nishi T and Ning N 2014 Graphene encapsulated rubber latex composites with high dielectric constant, low dielectric loss and low percolation threshold *J. Colloid Interface Sci.* **430** 249–56
- [5] Han X, Chen S, Lv X, Luo H, Zhang D and Bowen C R 2018 Using a novel rigid-fluoride polymer to control the interfacial thickness of graphene and tailor the dielectric behavior of poly(vinylidene fluoride-trifluoroethylene-chlorotrifluoroethylene) nanocomposites *Phys. Chem. Chem. Phys.* **20** 2826–37
- [6] Deng H, Lin L, Ji M, Zhang S, Yang M and Fu Q 2014 Progress on the morphological control of conductive network in conductive polymer composites and the use as electroactive multifunctional materials *Prog. Polym. Sci.* **39** 627–55
- [7] Feng Y, Deng Q, Peng C and Wu Q 2019 High dielectric and breakdown properties achieved in ternary BaTiO₃/MXene/PVDF nanocomposites with low-concentration fillers from enhanced interface polarization *Ceram. Int.* **45** 7923–30
- [8] Wang Y, Wang L, Yuan Q, Chen J, Niu Y, Xu X, Cheng Y, Yao B, Wang Q and Wang H 2018 Ultrahigh energy density and greatly enhanced discharged efficiency of sandwich-structured polymer nanocomposites with optimized spatial organization *Nano Energy* **44** 364–70
- [9] Zhou Y, Li Q, Dang B, Yang Y, Shao T, Li H, Hu J, Zeng R, He J and Wang Q 2018 A scalable, high-throughput, and environmentally benign approach to polymer dielectrics exhibiting significantly improved capacitive performance at high temperatures *Adv. Mater.* **30** 1805672
- [10] Yao L, Pan Z, Zhai J, Zhang G, Liu Z and Liu Y 2018 High-energy-density with polymer nanocomposites containing of SrTiO₃ nanofibers for capacitor application *Composites A* **109** 48–54
- [11] Liu F, Li Q, Li Z, Dong L, Xiong C and Wang Q 2018 Ternary PVDF-based terpolymer nanocomposites with enhanced energy density and high power density *Composites A* **109** 597–603
- [12] Pan Z, Yao L, Zhai J, Fu D, Shen B and Wang H 2017 High-energy-density polymer nanocomposites composed of newly structured one-dimensional BaTiO₃@Al₂O₃ nanofibers *ACS Appl. Mater. Interfaces* **9** 4024–33
- [13] Sun D, Chen F, Gao Y, Huang S and Wang Y 2019 Polymer-derived SiCN ceramics as fillers for polymer composites with high dielectric constants *J. Mater. Sci.* **54** 6982–90
- [14] Qu P, Zhu X, Peng X, Zhang M, Yang B and Liu X 2019 Ultrathin ceramic nanowires for high interface interaction and energy density in PVDF nanocomposites *Int. J. Appl. Ceram. Tech.* **16** 1200–8
- [15] Prateek, Bhunia R, Siddiqui S, Garg A and Gupta R K 2019 Significantly enhanced energy density by tailoring the interface in hierarchically structured TiO₂-BaTiO₃-TiO₂ nanofillers in PVDF-based thin-film polymer nanocomposites *ACS Appl. Mater. Interfaces* **11** 14329–39
- [16] Zhu Y, Yao H, Jiang P, Wu J, Zhu X and Huang X 2018 Two-dimensional high-k nanosheets for dielectric polymer nanocomposites with ultrahigh discharged energy density *J. Phys. Chem. C* **122** 18282–93
- [17] Tang C-W, Li B, Sun L, Lively B and Zhong W-H 2012 The effects of nanofillers, stretching and recrystallization on microstructure, phase transformation and dielectric properties in PVDF nanocomposites *Eur. Polym. J.* **48** 1062–72
- [18] Guan F, Pan J, Wang J, Wang Q and Zhu L 2010 Crystal orientation effect on electric energy storage in poly(vinylidene fluoride-co-hexafluoropropylene) copolymers *Macromolecules* **43** 384–92
- [19] Martins P, Costa C M, Benelmekki M, Botelho G and Lanceros-Mendez S 2012 On the origin of the electroactive poly(vinylidene fluoride) beta-phase nucleation by ferrite nanoparticles via surface electrostatic interactions *CrystEngComm* **14** 2807–11
- [20] Kim P, Doss N M, Tillotson J P, Hotchkiss P J, Pan M-J, Marder S R, Li J, Calame J P and Perry J W 2009 High energy density nanocomposites based on surface-modified BaTiO₃ and a ferroelectric polymer *ACS Nano* **3** 2581–92
- [21] Li Z, Liu F, Li H, Ren L, Dong L, Xiong C and Wang Q 2019 Largely enhanced energy storage performance of sandwich-structured polymer nanocomposites with synergistic inorganic nanowires *Ceram. Int.* **45** 8216–21
- [22] Pan Z, Yao L, Zhai J, Yao X and Chen H 2018 Interfacial coupling effect in organic/inorganic nanocomposites with high energy density *Adv. Mater.* **30** 1705662
- [23] Su R et al 2016 High energy density performance of polymer nanocomposites induced by designed formation of BaTiO₃@sheet-likeTiO₂ hybrid nanofillers *J. Phys. Chem. C* **120** 11769–76
- [24] Srivastava A, Maiti P, Kumar D and Parkash O 2014 Mechanical and dielectric properties of CaCu₃Ti₄O₁₂ and La doped CaCu₃Ti₄O₁₂ poly(vinylidene fluoride) composites *Compos. Sci. Technol.* **93** 83–9
- [25] Wang J, Xie Y, Liu J, Zhang Z and Zhang Y 2019 Towards high efficient nanodielectrics from linear ferroelectric P(VDF-TrFE-CTFE)-g-PMMA matrix and exfoliated mica nanosheets *Appl. Surf. Sci.* **469** 437–45
- [26] Peng X, Liu X, Qu P and Yang B 2018 Enhanced breakdown strength and energy density of PVDF composites by introducing boron nitride nanosheets *J. Mater. Sci.-Mater. Electron.* **29** 16799–804
- [27] Xie Y, Wang J, Yu Y, Jiang W and Zhang Z 2018 Enhancing breakdown strength and energy storage performance of PVDF-based nanocomposites by adding exfoliated boron nitride *Appl. Surf. Sci.* **440** 1150–8
- [28] Li W, Song Z, Qian J, Chu H, Wu X, Tan Z and Nie W 2018 Surface modification-based three-phase nanocomposites with low percolation threshold for optimized dielectric constant and loss *Ceram. Int.* **44** 4835–44
- [29] Gowdhaman P, Annamalai V and Thakur O P 2016 Piezo, ferro and dielectric properties of ceramic-polymer composites of 0–3 connectivity *Ferroelectrics* **493** 120–9
- [30] Wang K, Yiming W, Saththasivam J and Liu Z 2017 A flexible, robust and antifouling asymmetric membrane based on ultra-long ceramic/polymeric fibers for high-efficiency separation of oil/water emulsions *Nanoscale* **9** 9018–25

- [31] He D, Wang Y, Zhang L, Song S and Deng Y 2018 Poly (vinylidene fluoride)-based composites modulated via multiscale two-dimensional fillers for high dielectric performances *Compos. Sci. Technol.* **159** 162–70
- [32] Zhao B, Hamidinejad M, Zhao C, Li R, Wang S, Kazemi Y and Park C B 2019 A versatile foaming platform to fabricate polymer/carbon composites with high dielectric permittivity and ultra-low dielectric loss *J. Mater. Chem. A* **7** 133–40
- [33] Wu L, Wu K, Lei C, Liu D, Du R, Chen F and Fu Q 2019 Surface modifications of boron nitride nanosheets for poly (vinylidene fluoride) based film capacitors: advantages of edge-hydroxylation *J. Mater. Chem. A* **7** 7664–74
- [34] Pan Z, Liu B, Zhai J, Yao L, Yang K and Shen B 2017 NaNbO_3 two-dimensional platelets induced highly energy storage density in trilayered architecture composites *Nano Energy* **40** 587–95
- [35] Chen J, Wang X, Yu X, Yao L, Duan Z, Fan Y, Jiang Y, Zhou Y and Pan Z 2018 High dielectric constant and low dielectric loss poly(vinylidene fluoride) nanocomposites via a small loading of two-dimensional $\text{Bi}_2\text{Te}_3/\text{Al}_2\text{O}_3$ hexagonal nanoplates *J. Mater. Chem. C* **6** 271–9
- [36] Tong W, Zhang Y, Yu L, Luan X, An Q, Zhang Q, Lv F, Chu K P, Shen B and Zhang Z 2014 Novel method for the fabrication of flexible film with oriented arrays of graphene in poly(vinylidene fluoride-co-hexafluoropropylene) with low dielectric loss *J. Phys. Chem. C* **118** 10567–73
- [37] Ye H, Meng N, Xu C, Meng Z and Xin L 2018 High dielectric constant and low loss in poly(fluorovinylidene-co-hexafluoropropylene) nanocomposite incorporated with liquid-exfoliated oriented graphene with assistance of hyperbranched polyethylene *Polymer* **145** 391–401
- [38] Zhang K, Wang J, Subramanian R, Ye Z, Lu H and Yu Q 2007 Chain walking ethylene copolymerization with an ATRP inimer for one-pot synthesis of hyperbranched polyethylenes tethered with ATRP initiating sites *Macromol. Rapid Commun.* **28** 2185–91
- [39] Ye H, Lu T, Xu C, Han B, Meng N and Xu L 2018 Liquid-phase exfoliation of hexagonal boron nitride into boron nitride nanosheets in common organic solvents with hyperbranched polyethylene as stabilizer *Macromol. Chem. Phys.* **219** 1700482
- [40] Gorbachev R V *et al* 2011 Hunting for monolayer boron nitride: optical and Raman signatures *Small* **7** 465–8
- [41] Song L *et al* 2010 Large scale growth and characterization of atomic hexagonal boron nitride layers *Nano Lett.* **10** 3209–15
- [42] Guerra V, Wan C, Degirmenci V, Sloan J, Presvytis D and McNally T 2018 2D boron nitride nanosheets (BNNs) prepared by high-pressure homogenisation: structure and morphology *Nanoscale* **10** 19469–77
- [43] Ribeiro C, Costa C M, Correia D M, Nunes-Pereira J, Oliveira J, Martins P, Goncalves R, Cardoso V F and Lanceros-Mendez S 2018 Electroactive poly(vinylidene fluoride)-based structures for advanced applications *Nat. Protoc.* **13** 681–704
- [44] Martins P, Lopes A C and Lanceros-Mendez S 2014 Electroactive phases of poly(vinylidene fluoride): determination, processing and applications *Prog. Polym. Sci.* **39** 683–706
- [45] Belovickis J, Ivanov M, Svirskas Š, Samulionis V, Banys J, Solnyshkin A V, Gavrilov S A, Nekludov K N, Shvartsman V V and Silibin M V 2018 Dielectric, ferroelectric, and piezoelectric investigation of polymer-based P(VDF-TrFE) composites *Phys. Status Solidi b* **255** 1700196
- [46] He D, Wang Y, Song S, Liu S and Deng Y 2017 Significantly enhanced dielectric performances and high thermal conductivity in poly(vinylidene fluoride)-based composites enabled by SiC/SiO_2 core-shell whiskers alignment *ACS Appl. Mater. Interfaces* **9** 44839–46
- [47] Wu L, Wu K, Liu D, Huang R, Huo J, Chen F and Fu Q 2018 Largely enhanced energy storage density of poly(vinylidene fluoride) nanocomposites based on surface hydroxylation of boron nitride nanosheets *J. Mater. Chem. A* **6** 7573–84
- [48] Yang Y, He J, Li Q, Gao L, Hu J, Zeng R, Qin J, Wang S and Wang Q 2019 Self-healing of electrical damage in polymers using superparamagnetic nanoparticles *Nat. Nanotechnol.* **14** 151–5
- [49] Li Q, Chen L, Gadinski M R, Zhang S, Zhang G, Li H, Haque A, Chen L-Q, Jackson T N and Wang Q 2015 Flexible high-temperature dielectric materials from polymer nanocomposites *Nature* **523** 576–9
- [50] Wang Y, Cui J, Wang L, Yuan Q, Niu Y, Chen J, Wang Q and Wang H 2017 Compositional tailoring effect on electric field distribution for significantly enhanced breakdown strength and restrained conductive loss in sandwich-structured ceramic/polymer nanocomposites *J. Mater. Chem. A* **5** 4710–8
- [51] Wang C, Zhang J, Gong S and Ren K 2018 Significantly enhanced breakdown field for core-shell structured poly (vinylidene fluoride-hexafluoropropylene)/ TiO_2 nanocomposites for ultra-high energy density capacitor applications *J. Appl. Phys.* **124** 154103
- [52] Chen G, Lin X, Li J, Fisher J G, Zhang Y, Huang S and Cheng X 2018 Enhanced dielectric properties and discharged energy density of composite films using submicron PZT particles *Ceram. Int.* **44** 15331–7
- [53] Chen Y, Yao L, Yang C, Zhang L, Zheng P, Liu A and Shen Q-D 2018 In-depth understanding of interfacial crystallization via flash dsc and enhanced energy storage density in ferroelectric P(VDF-CTFE)/Au NRs nanocomposites for capacitor application *Soft Matter* **37** 7714–23
- [54] Pan Z, Wang M, Chen J, Shen B, Liu J and Zhai J 2018 Largely enhanced energy storage capability of a polymer nanocomposite utilizing a core-satellite strategy *Nanoscale* **10** 16621–9
- [55] Chi Q *et al* 2018 High energy storage density for poly (vinylidene fluoride) composites by introduced core-shell $\text{CaCu}_3\text{Ti}_4\text{O}_{12}/\text{Al}_2\text{O}_3$ nanofibers *ACS Sustain. Chem. Eng.* **6** 8641–9
- [56] Ye H, Zhang X, Xu C, Han B and Xu L 2018 Enhanced dielectric property and energy density in poly(vinylidene fluoride-chlorotrifluoroethylene) nanocomposite incorporated with graphene functionalized with hyperbranched polyethylene-graft-poly(trifluoroethyl methacrylate) copolymer *J. Mater. Chem. C* **6** 11144–55
- [57] Wang J, Hu J, Sun Q, Zhu K, Li B-W and Qiu J 2017 Dielectric and energy storage performances of PVDF-based composites with colossal permittivity Nd-doped BaTiO_3 nanoparticles as the filler *AIP Adv.* **7** 125104
- [58] Li S, Yu J, Yu S, Sun R, Cao L, Liao W-H and Wong C-P 2019 Significantly enhanced electrostatic energy storage performance of flexible polymer composites by introducing highly insulating-ferroelectric microhybrids as fillers *Adv. Energy Mater.* **9** 1803204
- [59] Dou Z, Liu W, Lin T, Zhou K and Huang L 2017 High performance capacitors via aligned TiO_2 nanowire array *Appl. Phys. Lett.* **110** 133902
- [60] Zheng M-S, Zha J-W, Yang Y, Han P, Hu C-H and Dang Z-M 2016 Enhanced breakdown strength of poly(vinylidene fluoride) utilizing rubber nanoparticles for energy storage application *Appl. Phys. Lett.* **109** 072902
- [61] Pan Z, Yao L, Zhai J, Shen B, Liu S, Wang H and Liu J 2016 Excellent energy density of polymer nanocomposites containing $\text{BaTiO}_3/\text{Al}_2\text{O}_3$ nanofibers induced by moderate interfacial area *J. Mater. Chem. A* **4** 13259–64